Surface Structures of a-Fe$_2$O$_3$(0001) Phases determined by LEED Crystallography

G. Ketteler[1], W. Weiss, W. Ranke[*]

Department of Inorganic Chemistry, Fritz-Haber-Institute of the MPG, Faradayweg 4-6, 14195 Berlin, Germany

[1] Also: FU Berlin, Fachbereich Biologie, Chemie, Pharmazie, Takustr. 3, 14195 Berlin, Germany.

[*] Corresponding author: e-mail ranke@fhi-berlin.mpg.de, phone +49 30 8413 4523, fax +49 30 8413 4401

Abstract

We present a dynamical Tensor low-energy electron diffraction (LEED) study of α-Fe$_2$O$_3$(0001) surface structures forming in an oxygen pressure range from 10^{-5} to 1 mbar. Epitaxial α-Fe$_2$O$_3$(0001) films were prepared on Pt(111) in defined oxygen partial pressures at temperatures around 1100K. In 1 mbar O$_2$, strongly relaxed oxygen terminated surface structures are formed while in 10^{-5} mbar O$_2$ three different surface structures yield rather good Pendry R-factors. Further experimental evidence from scanning tunneling spectroscopy (STM) and ion scattering spectroscopy (ISS) in combination with a critical review of the literature is only consistent with a hydroxyl termination forming in 10^{-5} mbar O$_2$. The stabilization of both structures is discussed on the basis of electrostatic arguments considering the boundary conditions at the oxide/gas as well as oxide/substrate interface (autocompensation). For oxygen pressures between 10^{-4} to 10^{-1} mbar O$_2$, both domains coexist as analyzed using a new, modified version of the symmetrized automated Tensor LEED program package.

The system investigated in this study turns out to be very complex and the LEED analysis alone is not capable to identify the involved surface structures unambiguously. Only in combination with results from other surface sensitive methods it was possible to deduce models for the most likely surface structures.

1. Introduction

The ultra-high vacuum (UHV) approach to the study of catalytic materials offers many advantages over traditional methods in that a variety of modern surface science techniques are available to determine the structure and composition and to identify relevant surface species of surfaces on an atomic level.[1,2] On the other hand, catalytic reactions are typically performed at atmospheric or even higher pressures with catalysts possessing complex structures. Not much is known about how the chemical properties of a catalyst change across a pressure range from ultra-high vacuum to atmospheric conditions („pressure gap„). Therefore, systematic investigations in this pressure range are necessary since the structure of compounds at thermodynamic equilibrium depends strongly on the ambient gas pressure,[3,4] and it may therefore change across the pressure gap leading to materials with different catalytic properties.[5]

Iron oxides are important materials that are used as heterogenous catalysts for various reactions. For instance, potassium promoted iron oxides are used in the dehydrogenation of ethylbenzene to styrene in presence of steam.[6-9] During the last years, clean and well-ordered iron oxide films have been prepared by iron deposition onto chemically inert metal substrates and subsequent oxidation at temperatures of 900-1100K.[10-11] These films can be prepared with defined composition and surface termination depending on the preparation conditions which are determined by equilibrium thermodynamics.[4] In order to transform heteroepitaxially grown Fe$_3$O$_4$(111) films to α-Fe$_2$O$_3$(0001), temperatures around 1100K and oxygen partial pressures above 10^{-5} mbar are necessary.[4,12] For such conditions, two different surface terminations are observed in atomic resolution scanning tunneling microscopy (STM) images dependent on the ambient oxygen gas pressure during annealing.[12] On the basis of ab initio spin-density functional theory calculations these have been assigned to an unreconstructed and strongly relaxed α-Fe$_2$O$_3$(0001) surface structure terminated by an outermost oxygen layer in high oxygen pressures and a strongly relaxed iron-terminated surface structure in low oxygen pressure environments,[13] although no direct experimental evidence for this assignment exists. According to the autocompensation principle, polar surfaces as for example an oxygen-terminated α-Fe$_2$O$_3$(0001) surface should not be stable,[14] and X-ray photoelectron diffraction measurements of MBE-grown epitaxial α-Fe$_2$O$_3$(0001) films revealed a strongly relaxed iron termination to be stable even after

Surface Structures of α-Fe2O3(0001) Phases determined by LEED Crystallography, G. Ketteler et al., Surf. Rev. Lett. 8 (2001), 661.

2

cooling to room temperature in highly oxidizing oxygen plasma.[15] Nevertheless, several ways to reduce the dipole moment of polar surfaces have been proposed by means of relaxations, reconstructions or charged adsorbates,[16-19] and especially in the case of thin, epitaxially grown films, the boundary condition to the substrate may have a stabilizing effect so that also an oxygen termination is proposed to be stable.[19] A recent study of NiO(111) proposed that thin, octopolar reconstructed NiO(111) films also exhibit two terminations which are Ni- and O-terminated.[20]

In this study, the surface structures of α-Fe$_2$O$_3$(0001) in dependence of the oxygen pressure as observed in the STM analysis by Shaikhutdinov and Weiss[12] are determined by dynamical LEED analysis. All LEED intensity-voltage (I-V-) curves presented in this paper were recorded immediately before or after STM investigations which led to STM images as presented by these authors.

2. Experimental and Calculation Procedure

2.1. Experimental

The experiments were performed in an ultra-high-vacuum (UHV) chamber with a base pressure of 1×10^{-10} mbar. As described in detail in reference,[21] this chamber is equipped with a commercial STM head (Burleigh Instruments), back-view LEED optics (Omicron) and a cylindrical mirror analyzer for Auger electron spectroscopy (Omicron). An ion bombardment gun and several gas inlet valves are also present. The platinum crystal could be heated by electron bombardment from the back and cooled by a liquid nitrogen reservoir. The high-pressure oxidation was performed in a separate preparation cell using a radiation heater that provides sample temperatures around 1130K in oxygen partial pressures up to 10 mbar. The transfer from and to this preparation cell can be performed under ultra-high vacuum conditions.

The Pt(111) surface was prepared by repeated cycles of argon ion bombardment and subsequent annealing to 1300 K until it exhibited a sharp (1x1) LEED pattern and no contamination signals in the Auger electron spectrum. Well-ordered Fe$_3$O$_4$(111) magnetite films several hundred Å thick were grown by repeated cycles of iron deposition and subsequent oxidation in 10^{-6} mbar oxygen at ~1000K.[22] The Fe$_3$O$_4$(111) magnetite films can be transformed into well-ordered α-Fe$_2$O$_3$(0001) films by a high-pressure oxidation at temperatures above 1100K and oxygen pressures higher than 10^{-3} mbar in order to induce the bulk structural transformation from Fe$_3$O$_4$ to α-Fe$_2$O$_3$ within reasonable time (a few minutes). This was done in the separate preparation cell which has a base pressure of about 5×10^{-8} mbar. After the oxidation process, the oxygen was pumped off when the sample temperature dropped below ~600K and the sample was transferred back into the analysis chamber. In order to produce surfaces at pressures below 10^{-3} mbar, the films were first oxidized above 10^{-3} mbar and then the pressure was reduced to 10^{-4} to 10^{-6} mbar. Then, the films were transferred back to the main chamber. The time between the final anneal in the preparation chamber and the start of STM or LEED measurements was at least 30 minutes.

For oxygen pressures between 1 mbar and 10^{-5} mbar, similar α-Fe$_2$O$_3$(0001)-(1x1) LEED patterns similar to that shown in fig. 1 and similar Auger spectra were observed. The LEED pattern always exhibits six-fold symmetry due to the coexistence of equally terminated domains which are rotated by 180° by each other. Reducing the oxygen partial pressure during annealing to 10^{-6} mbar results in a partial reduction of the surface and a superstructure of ordered domains of Fe$_{1-x}$O(111) and α-Fe$_2$O$_3$(0001) is formed similar to the structure called 'biphase ordering' observed by Condon et al.[23]
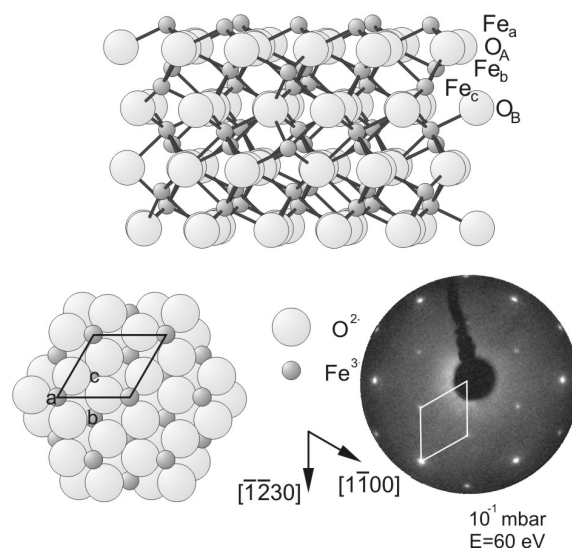

Fig. 1: Side and top views of the bulk structure of α-Fe$_2$O$_3$(0001) and the corresponding LEED pattern (E = 60 eV).
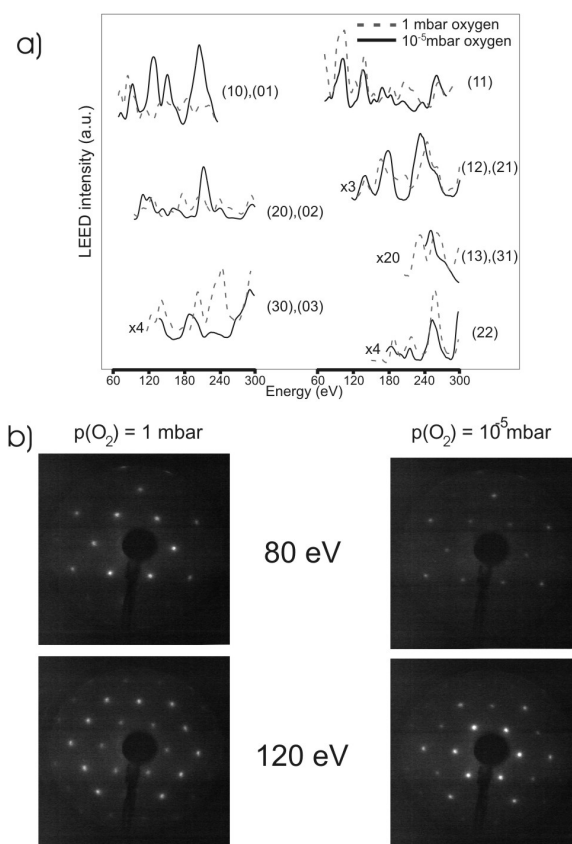

Fig. 2: (a) Comparison of LEED I-V spectra for α-Fe$_2$O$_3$(0001) films prepared in 1 mbar and 10^{-5} mbar O$_2$. (b) LEED images at 80 eV and 120eV.

Except where indicated, the LEED measurements were performed at a sample temperature of T=120 K which was achieved by cooling with liquid nitrogen. Intensity-Voltage (I-V) curves were measured at normal incidence. The diffraction patterns were recorded with a CCD camera from the backview LEED screen and stored via a VMEbus computer onto a workstation hard disk (ultra sparc 2). Noise reduction was possible by averaging up to 255 images. For extraction of the I-V curves these images were processed with software programs developed at the Fritz-Haber-Institute. The LEED I-V characteristic of films prepared in 10^{-5} mbar and 1 mbar O$_2$ deviate significantly as shown in fig. 2. The reproducability of the I-V spectra for films prepared in 10^{-5} and 1

Surface Structures of α-Fe2O3(0001) Phases determined by LEED Crystallography, G. Ketteler et al., Surf. Rev. Lett. 8 (2001), 661.

3

mbar O_2 is good. The R-factor calculated from comparison of two identically prepared experimental I-V spectra is below 0.07 while comparing films prepared in 10^{-5} mbar and 1 mbar O_2 yields R-factors >0.65. In order to quickly distinguish both surface structures one may take LEED images at energies of 80 and 120eV as shown in fig. 2(b). At these energies, the intensity ratio between the (10) and (11) beams serves to distinguish between the different terminations.

2.2. LEED calculations

The LEED calculations were performed on an ultra sparc 2 workstation using the Barbieri/Van Hove Symmetrized Automated Tensor LEED (SATLEED) package[24] and a modified version. The theory of this perturbation method was mainly developed by Rous et al.,[25] and a detailed computational description is given in reference.[26] In a first step a full dynamical calculation is performed for a chosen reference structure including the quantities needed to construct the tensor. With this tensor, I-V-curves for a variety of models in the proximity of the reference structure can be calculated approximately with little cost in computer time. The search for the best structure model was performed by an automated algorithm, where the agreement between theoretical and experimental I-V curves was quantified by the Pendry-R-factor.[27] Because the tensor calculations are perturbative, care has to be taken if atomic coordinates in the optimized model deviate from the starting reference structure by more than about 0.1 Å, depending somewhat on the number of parameters. In this case a new reference structure with the geometry of the optimized model has to be defined, again a full dynamical calculation has to be performed, followed by the tensor search in the proximity of this new reference structure. This procedure was repeated until the final structure obtained by the tensor search deviated by less than a few hundredths of an Ångström from the last reference structure. In order to rule out alternative models that reveal higher R-factors, the variance at the R-factor minimum of the best fit structure ΔR was used as a confidence interval, where ΔR is calculated under the assumption of random, non-correlated errors.[27] Since large relaxations have to be expected for a polar metal oxide surface such as α-Fe2O3(0001), a large number of reference structure calculations with a subsequent search for an R-factor minimum in the vicinity of each reference structure has to be performed for all possible surface terminations. For this, a shell script was written which automatically creates reference structures with geometries varied in systematic ways as described in section 3B.

The scattering phase shifts were taken from reference.[28] These have been calculated for Fe^{2+} and O^{2-} ions in the FeO sodium chloride structure. All (0001) layers in the α-Fe2O3 structure are separated by less than 1 Å, the distance between two adjacent iron layers is 0.595 Å and the distance between one oxygen and the adjacent iron layers is 0.846 Å. This is too close to ensure convergence of the multiple scattering computations between these layers. Therefore we defined a composite layer consisting of 20 atomic layers corresponding to one three-dimensional unit cell of α-Fe2O3. The search for the best structure was performed with phase shifts for angular quantum numbers l=6, a temperature of calculation of 120K, and a Debye temperature of 300 K for oxygen and 550 K for iron. It was checked that this number of phase shifts led to no loss in accuracy when compared with more phase shifts. The imaginary part of the inner potential V_{0i} was fixed to a value of -5 eV, the real part V_0 was fitted within each calculation starting from a value of 5 eV. In the final refinement of the best structure, the number of phase shifts was increased from $l_{max}=6$ to 8, and the imaginary part of the inner potential as well as the Debye temperatures for both iron and oxygen atoms were optimized.

In order to determine the structure of mixed terminated films, the program code of the SATLEED program package was modified. The program code of version 4 of the Barbieri/Van Hove program package was left mainly untouched. Program part 1 which calculates the tensors was not changed at all, i.e. the tensors have to be calculated separately for each termination. From these tensors the diffraction matrices of the model structures were calculated as in the standard version, and just before the R-factor for the model structures would be generated, the diffraction matrices of all terminations are incoherently mixed by a weighting factor which has to be provided by the input file rfac.e. The program enables mixing of several different terminations and of several data sets recorded for different angles of inciidence. For details of the FORTRAN program code we refer to the comments in the program files which can be ordered from M. A. Van Hove.[24]

Since the tensors are calculated separately for each termination, only terminations expanding over rather large surface areas can be treated by this program code. In other words: Multiple diffraction paths from one termination to another are not considered leaving a general uncertainty in the calculation (incoherent mixing). For large domain sizes this is neglible, nevertheless in case the differently terminated domains are small, the ratio of domain boundaries to domain area becomes large and such multiple diffraction paths contribute to a large extent to the I-V characteristic. We presume that this program code is not applicable in this case.

The modified program code always considers a larger number of parameters to be optimized in the iteration procedures. This always leads to an improvement of the fit which is not necessarily due to structural improvements. A criterion to test whether the improvement is significant was suggested by Hamilton for X-ray crystallography:[29,30]

$$H_r = \frac{\left(R_s^2 - R_{mix}^2\right)(n-p)}{R_{mix}^2(p-q)}$$

with R_s and R_{mix} R-factors for the model with smaller (q) and larger (p) number of fitting parameters, n = number of experimental data points. The number of experimental data points can be estimated from the total energy range and the peak width which is about $2|V_{0i}|$. A large ratio indicates real improvements (as long as the structural coordinates are otherwise reasonable), exceeding a value of 3 was found to be sufficient.[31] The MSATLEED program code and the Hamilton ratio have been succesfully applied to an extensive LEED analysis of the α-Al2O3(0001) surface structure.[31]

3. Results

3.1. Bulk a-Fe2O3(0001) crystal structure

α-Fe2O3 (hematite) is the only binary iron oxide phase that is stable at room temperature at thermodynamic equilibrium.[4] It crystallizes in the corundum structure with a hexagonal unit cell containing six formula units. The lattice constants are a=5.035 Å and c=13.72 Å.[32] The oxygen anions form a hcp sublattice with only octahedrally coordinated Fe^{3+} species located in interstitial sites. Along the crystal c-axis the hexagonal oxygen (0001) planes form an ABAB stacking sequence with two iron sublayers inbetween. The interatomic distance within these iron layers is 5.03 Å, which corresponds to the lattice constant of the two-dimensional unit cell of an unreconstructed (0001) surface, as indicated in the top view of fig. 1. The oxygen anion postitions within the (0001) planes also deviate somewhat from an ideal hexagonal arrangement, leading to an average oxygen-oxygen interatomic distance of 2.91Å. There are two different iron-oxygen bond lengths, 1.96 Å and 2.09 Å, as the iron cations form distorted octahedrons with their oxygen neighbors in the hematite structure. The average oxygen-oxygen intera-

tomic distance within one layer is 2.91Å. Ionic radii of Fe^{3+} and O^{2-} are 0.64 Å and 1.32 Å, respectively.[33] The two iron subplanes in between the oxygen planes are vertically 0.6 Å apart. The distance between two oxygen planes is 2.29 Å, which corresponds to the distance between equivalent (0001) surface terminations of α-Fe_2O_3.

3.2. Search for the best fit structure

I-V curves were recorded at normal incidence, therefore they are more sensitive to the interlayer distance than to the atomic positions parallel to the surface.[34] The aim of the first optimization steps was the determination of the atomic layer sequence and the first interlayer distances for the nearly single terminated surface structures forming in 1 mbar and 10^{-5} mbar O_2, respectively, since the atomic layers in α-Fe_2O_3(0001) are very closely spaced and large relaxations of the interlayer distances are quite common for oxide surfaces. Furthermore, for similar oxide surface structures like the isostructural Cr_2O_3(0001)[35] as well as Fe_3O_4(111)[36] permutations of the layer sequence were recently proposed and therefore stacking faults have to be considered. The tested layer sequences are shown in table I which summarizes the first optimization step for the structure forming in 10^{-5} mbar. Column two shows the layer sequences of the tested structural models. The different iron oxygen sublayers are abbreviated by symbols Fe_a, Fe_b, Fe_c and O_A, O_B as shown in the side view of α-Fe_2O_3(0001) in fig. 1. The subscripts denote the lateral position of the atoms as indicated in the top view of fig. 1. For the corundum structure three energetically inequivalent bulk cleavage terminations are possible: a single iron termination, a double iron termination and an oxygen termination. All these possible structure models have to be considered in the search. Models 1-3 are the three energetically inequivalent bulk truncations, and only the layer sequence which yielded the best agreement of experiment and theory is shown in table I. Models 4 and 5 correspond to an iron termination with a lateral shift of the topmost iron layer (corresponding to a stacking fault of the iron layer sequence). Model 6 is an oxygen capped iron termination, i.e. the topmost iron layer is tetrahedrally saturated by oxygen atoms. Model 7 corresponds to an oxygen capped double iron termination and model 8 shows a stacking fault where three (instead of two) iron layers are in between the

two topmost oxygen layers. The layer sequence of this model is similar to the one recently proposed for α-Cr_2O_3(0001).[35] For all these stucture models, the first three interlayer distances were varied systematically from 0 to 150% of its bulk value in steps of 0.15Å to create the different reference structures. Only atomic coordinates perpendicular to the surface were allowed to relax in a first optimization step. 13 atomic coordinates (7 layers) corresponding to a thickness of approximately 3.5Å were allowed to relax in this first step. Structural models deviating by more than the variance ΔR from the best R-factor (see above) were ruled out from further optimization steps. In a next step, lateral relaxations for these layers were allowed under the constraint of symmetry conservation. Often, atomic coordinates shifted by more than 0.1Å making another full dynamical calculation necessary. Optimization of 20 atomic parameters (13 layers) or even 30 parameters (20 layers) perpendicular to the surface yielded no significant improvement of the data while allowing lateral relaxations decreased the R-factor significantly. The increase of fitting parameters, however, may lead to a decrease of the R-factor which is simply due to the increased number of fitting parameters and has no physical origin as discussed in section 2.2. In order to check the maximum number of reliable parameters we applied the Hamilton test ratio introduced in section 2.2. Plots where the decrease of the Pendry R-factor (solid curves in figs. 3(d-f)and 4(c),(d)) with increasing number of parameters were compared to the minimum R-factor which would be expected for a Hamilton ratio of 3 (dashed curves) were included in sections 3.3 and 3.4 to estimate how many parameters give reliable results. The solid curves have to be below the dashed ones to indicate a reliable improvement. The plots show that for the high pressure models described in detail in section 3.4, more than 7 parameters do not produce a significant improvement of the R-factor while in case of the low pressure model structure described in section 3.3, also the variation of 20 atomic parameters gives reliable improvements with Hamilton ratios around 3.

In a last step the Debye temperatures and the inner potential were optimized for the best fit structures.

Table I: Tested layer sequences and Pendry R-Factors after the first optimization step for the surface structure forming in 10^{-5} mbar O_2. The layer sequence of all structural models is abbreviated in column 2 by numbers which denote the number of atoms per 2D-unit cell and by subscripts as introduced in fig. 1. For details see text.

#	Layer sequence	# structure models tested	R_P for best model
1	$3O_A$-$1Fe_b$-$1Fe_c$-$3O_B$-$1Fe_a$-$1Fe_{b-...}$	100	0.33
2	$1Fe_a$-$3O_A$-$1Fe_b$-$1Fe_c$-$3O_B$-$1Fe_{a-...}$	180	0.40
3	$1Fe_c$-$1Fe_a$-$3O_A$-$1Fe_b$-$1Fe_c$-$3O_{B-...}$	150	0.39
4	$1Fe_b$-$3O_A$-$1Fe_b$-$1Fe_c$-$3O_B$-$1Fe_{a-...}$	60	0.42
5	$1Fe_c$-$3O_A$-$1Fe_b$-$1Fe_c$-$3O_B$-$1Fe_{a-...}$	60	0.40
6	$1O_a$-$1Fe_a$-$3O_A$-$1Fe_b$-$1Fe_c$-$3O_{B-...}$	200	0.36
7	$1O_c$-$1Fe_c$-$1Fe_a$-$3O_A$-$1Fe_b$-$1Fe_{c-...}$	240	0.36
8	$1Fe_c$-$3O_A$--$1Fe_b$-$1Fe_a$-$1Fe_c$-$3O_{B-...}$	96	0.37

3.3. Surface structure forming in 10^{-5} mbar oxygen pressure

The first optimization step for the surface structure forming in 10^{-5} mbar O_2 is summarized in table I. The Pendry R-Factor is included in the last column for the structural

model which gives the best fit between experiment and theory without further optimization (i.e. that in some cases, deviations of atomic coordinates by more than 0.1Å occur which would make a full dynamical calculation for this structure necessary). One can see that in general structural

Surface Structures of α-Fe2O3(0001) Phases determined by LEED Crystallography, G. Ketteler et al., Surf. Rev. Lett. 8 (2001), 661.

5

models terminated by oxygen atoms (models 1,6,7) reveal a better agreement between experiment and theory. Since even the layer sequence remains unclear after this first optimization step, we included one further optimization step where we varied the 4th to 6th layer distances in a systematic manner in steps of 0.1 Å around their bulk value. 28 structure models remained after this second optimization step and still none of the 8 layer sequences could be unambigiously identified. In a third step, also lateral relaxations

were allowed for 7 layers and then also for 13 and all 20 atomic layers. The atomic coordinates of these layers were optimized until deviations of only a few hundredth Å remained. Some of the structures evolved into the same local minimum while others could not be located. Finally, we ended up with three structural models shown in table II. The Pendry-R-factors of all other structural models is ≥0.30.
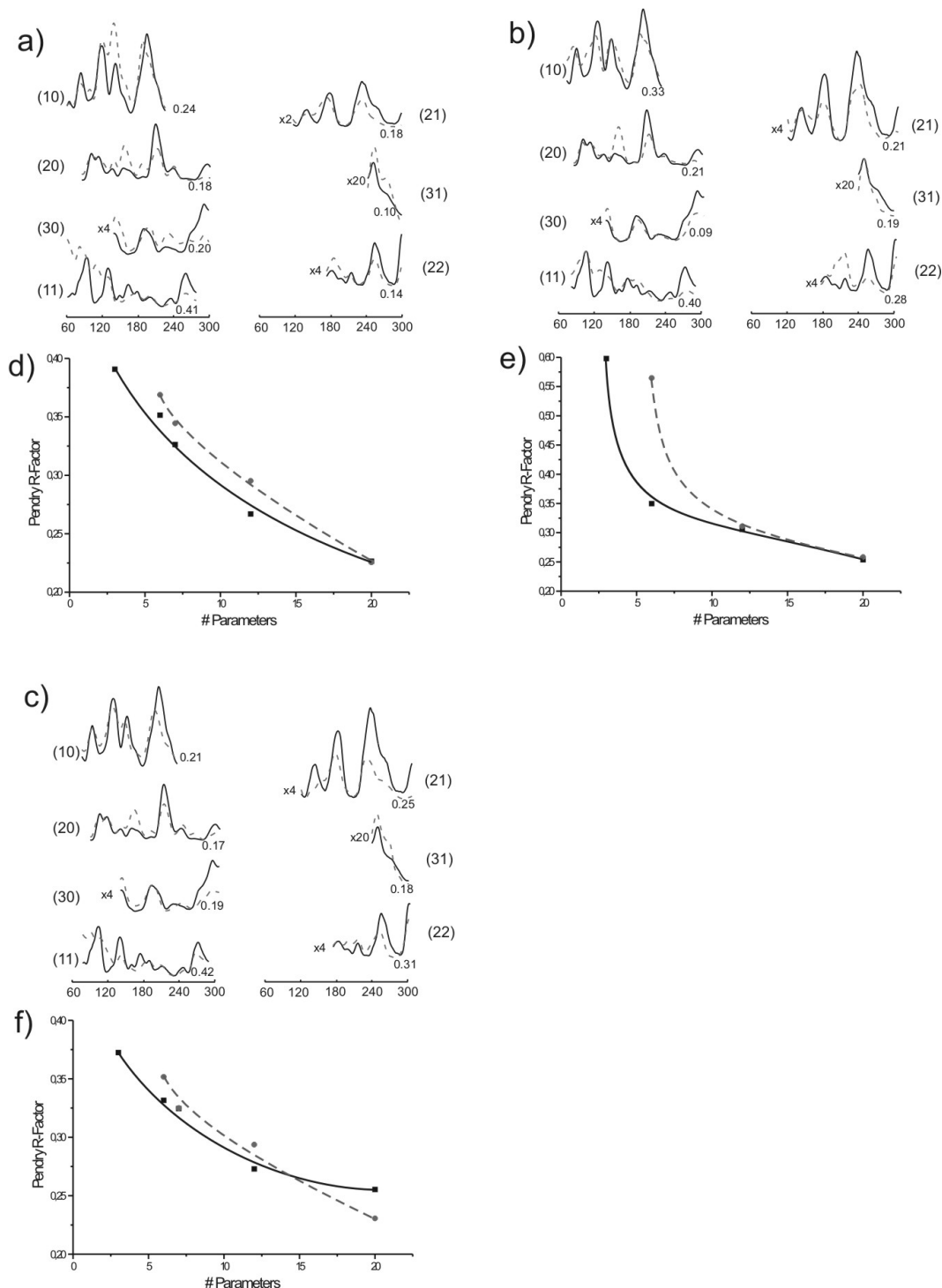

Fig. 3: (a) LEED I-V spectra for the surface structure model which gives the best fit between experimental (solid curves) and theoretical (dashed curves) I-V curves for the film forming in 10^{-5} mbar O_2 (R_P = 0.227). (b) LEED I-V spectra for the surface structure model which gives the second-best fit between experimental (solid lines) and theoretical (dashed lines) I-V curves for the film forming in 10^{-5} mbar O_2 (R_P = 0.254). (c) LEED I-V spectra for the surface structure model which gives the third-best fit between experimental (solid lines) and theoretical (dashed lines) I-V curves for the film forming in 10^{-5} mbar O_2 (R_P = 0.255). The Pendry R factors for the single beams are also indicated. (d)-(f) Decrease of the Pendry R factor in dependence of the atomic parameters allowed to relax (solid curves) compared to the minimum values expected for a physically meaningful improvement (dashed curves). For details see text.

Surface Structures of α-Fe2O3(0001) Phases determined by LEED Crystallography, G. Ketteler et al., Surf. Rev. Lett. 8 (2001), 661.

6

Figure 3 compares the decrease of the Pendry R-factor for allowing increasing numbers of parameters to be optimized with the maximum R-factors calculated for a Hamilton ratio of 3. These plots show whether the improvement by allowing more parameters to relax is physically significant or just due to the increased numbers of fitting parameters. In case the dashed curves are above the solid lines, the improvement is significant. This is the case for the oxygen (fig. 3(d)) and iron terminated model (fig. 3(e)) but not for the double iron terminated model (fig. 3(f)). A reliable double terminated surface can only be achieved when not more than 13 parameters were allowed to relax, this yields a Pendry R-factor of 0.29 and can thus be clearly ruled out. Furthermore, bond lengths in this structure are extremely short (Fe-O distances between 1.63 and 2.53Å and O-O distances between 2.14 and 3.11 Å, the overlap of the ionic radii would thus be >0.5Å) and no experimental or theoretical work supports the formation of a double iron terminated surface for compounds M_2O_3 with corundum structure. For these reasons, we excluded this model.

Table II: Pendry R-factor and interlayer distances for the best fit structural models for the film prepared in 10^{-5} mbar O_2.

	#1	#2	#3
Fe_c	-	-	-53%
Fe_a	-	-79%	-23%
$3O_A$	+10%	+4%	+7%
Fe_b	+28%	+35%	+8%
Fe_c	-24%	-28%	-4%
R_{Pendry}	0.227	0.254	0.255

The best agreement between experimental and theoretical I-V spectra is obtained for an oxygen terminated surface structure (model #1 in table II). The Pendry R-Factor of 0.227 is quite good, only the (11) beam yields a poor Pendry R-Factor of 0.407 (fig. 3(a)). This beam has the largest contribution from 1st order scattering at the oxygen sublattice (although, of course, all scattering paths contribute due to multiple scattering effects), and thus may be due to defects in the oxygen sublattice. The role of oxygen vacancies is discussed in section 4. This structure exhibits an outward relaxation of the first two layer distances of 10% and 28%, respectively (tables II, III). The third layer distance is contracted by 24%. The distance between the first and second oxygen layer is unchanged within the error bars. The lateral oxygen positions in this structure are shifted with respect to bulk α-Fe2O3, the trigonal symmetry of the (0001) layers is preserved. The Fe-O distances are between 1.62 and 2.44Å, and the O-O distances fall between 2.38 and 3.29 Å. The short interatomic O-O distances of 2.38A correspond to an overlap of 0.24A of the ionic radii. The lateral displacements of the oxygen atoms yielded an improvement of the Pendry R-factor from 0.314 to 0.227 which is unlikely to be exclusively due to the higher number of fitting parameters in the optimization. The interlayer distances are not affected upon lateral relaxation of the oxygen atoms. Large lateral relaxations as well as relaxations perpendicular to the surface occur even for layers which are rather far away from the surface. The optimized Debye temperatures are 600K for Fe and 550K for O, and the optimized imaginary as well as the real part of the inner potential is –7eV.

A strongly relaxed iron terminated structure model yields a Pendry R-factor of 0.254 (model #2 in table II). The I-V spectra are shown in fig. 3(b). The first layer distance is contracted by 79%. The second and third layer distances are expanded by 4 and 35%, respectively. Also in this case, lateral displacements of the oxygen atoms with respect to the bulk positions occur (table IV). The Fe-O distances in this structure are between 1.81 and 2.38Å and all O-O distances are between 2.20 and 3.33Å. The Fe-O distances are reasonable but O-O distances of 2.20Å result in a huge overlap of the ionic radii. We ended up with Debye-Temperatures of 275K for Fe and 350K for O. The real part of the inner potential is 5.3eV and the imaginary part is –6eV.

Table III: Atomic coordinates (in Å) for the α-Fe2O3(0001) bulk structure and for the surface structure model which gives the best fit between experimental and theoretical I-V curves for the film forming in 10^{-5} mbar O_2 (R_P=0.227).

Layer	Atom	surface structure (optimized)			bulk structure (crystal structure)		
		z	x	y	z	x	y
1	O	-0.888	-0.091	-1.636	-0.846	-0.145	-1.762
1	O	-0.888	-1.372	0.897	-0.846	-1.454	1.007
1	O	-0.888	1.462	0.739	-0.846	1.599	0.755
2	Fe	0.041	0.000	0.000	0.000	0.000	0.000
3	Fe	0.803	-1.454	-2.518	0.5945	-1.454	-2.518
4	O	1.448	-1.287	-0.700	1.441	-1.308	-0.755
4	O	1.448	0.037	1.464	1.441	0.000	1.511
4	O	1.448	1.250	-0.766	1.441	1.308	-0.755
5	Fe	2.319	1.454	2.518	2.287	1.454	2.518
6	Fe	2.945	0.000	0.000	2.881	0.000	0.000

Table IV: Atomic coordinates (in Å) for the α-Fe$_2$O$_3$(0001) bulk structure and for the surface structure model which gives the second best fit between experimental and theoretical I-V curves for the film forming in 10^{-5} mbar O$_2$ (R$_P$=0.254).

Layer	Atom	surface structure (optimized)			bulk structure (crystal structure)		
		z	x	y	z	x	y
1	Fe	-1.123	1.454	2.518	-1.692	1.454	2.518
2	O	-0.948	-0.184	-1.564	-0.846	-0.145	-1.762
2	O	-0.948	-1.263	0.941	-0.846	-1.454	1.007
2	O	-0.948	1.446	0.633	-0.846	1.599	0.755
3	Fe	-0.067	0.000	0.000	0.000	0.000	0.000
4	Fe	0.736	-1.454	-2.518	0.5945	-1.454	-2.518
5	O	1.342	-1.431	-0.729	1.441	-1.308	-0.755
5	O	1.342	0.084	1.604	1.441	0.000	1.511
5	O	1.342	1.347	-0.875	1.441	1.308	-0.755
6	Fe	2.182	1.454	2.518	2.287	1.454	2.518
7	Fe	2.874	0.000	0.000	2.881	0.000	0.000

3.4. Surface structure forming in 1mbar oxygen pressure

For this film, the tested structural models after a first optimization step without further refining are shown in table V. After the first optimization step, only oxygen-terminated models remained (regular oxygen termination #1 and the two oxygen-capped iron and double iron terminations #6 and #7). After the second optimization step, two models could be unambigiously identified while all other models deviated by more than the variance ΔR (see table VI). These models were refined in the last optimization steps and the coordinates of the resulting structures are shown in table VII and VIII. As discussed in section 3B, we found that allowing more than 7 atomic parameters to relax led to a decrease of the Pendry-R factor which is only due to the increased number of fitting parameters and thus is not physically meaningful. The Pendry R-factors of the two structures are 0.381 and 0.408, respectively. The LEED I-V spectra are shown in fig. 4(a),(b). The high value of the overall Pendry R-factor may be caused by the following reasons: Similar to the films prepared in 10^{-5} mbar O$_2$, the LEED images reveal a high background intensity, especially at high energies. Furthermore, STM images of films prepared in 1mbar O$_2$ always showed that the film is not entirely single-terminated but up to 10% of the other termination is present in form of small domains on the surface.[12] As will be shown below, the R-factor decreases slightly for this data set when 5-10% of the IV spectra of the best-fit low-pressure model is mixed (see fig.7(a)).

Table V: Tested layer sequences and Pendry R-Factors after the first optimization step for the surface structure forming in 1 mbar O$_2$. The layer sequence of all structural models is abbreviated in column 2 by numbers which denote the number of atoms per 2D-unit cell and by subscripts as introduced in fig. 1.

#	Layer sequence	# structure models tested	R$_P$ for best model
1	3O$_A$-1Fe$_b$-1Fe$_c$-3O$_B$-1Fe$_a$-1Fe$_b$-...	180	0.39
2	1Fe$_a$-3O$_A$-1Fe$_b$-1Fe$_c$-3O$_B$-1Fe$_a$-...	120	0.48
3	1Fe$_c$-1Fe$_a$-3O$_A$-1Fe$_b$-1Fe$_c$-3O$_B$-...	80	0.46
4	1Fe$_b$-3O$_A$-1Fe$_b$-1Fe$_c$-3O$_B$-1Fe$_a$-...	60	0.49
5	1Fe$_c$-3O$_A$-1Fe$_b$-1Fe$_c$-3O$_B$-1Fe$_a$-...	60	0.52
6	1O$_a$-1Fe$_a$-3O$_A$-1Fe$_b$-1Fe$_c$-3O$_B$-...	100	0.43
7	1O$_c$-1Fe$_c$-1Fe$_a$-3O$_A$-1Fe$_b$-1Fe$_c$-...	175	0.43
8	1Fe$_c$-3O$_A$--1Fe$_b$-1Fe$_a$-1Fe$_c$-3O$_B$-...	96	0.52

Table VI: Pendry R-factor and interlayer distances for the best fit structural models for the film prepared in 1 mbar O$_2$.

	#1	#2
Fe$_c$	-	-
Fe$_a$	-	-
3O$_A$	-46%	-1%
Fe$_b$	+46%	-95%
Fe$_c$	0%	+35%
R$_{Pendry}$	0.381	0.408

The first interlayer distance in the best fit structure is contracted by 46% and the second one is expanded by 45%. Lateral displacements of oxygen atoms are shown in tableVII. The Fe-O distances are between 1.68 and 2.32Å, and the O-O distances are between 2.46 and 2.94Å. The optimized Debye temperatures are 700 K for Fe and 450 K for O. The optimized imaginary part of the inner potential is –9 eV and the real part is 10.8 eV.

The first interlayer distance in the second best fit structure is contracted by 1% and the second one is contracted by 95%. The latter means that within the error bars both iron layers underneath the first oxygen layer have moved into one plane while the distances between oxygen layers are approximately the same as in the bulk structure. The trimers of oxygen atoms in the first layer are rotated by 3° as shown in fig. 4(f) leading to a more homogenous distribution of the oxygen atoms in this layer. Lateral displacements of oxygen atoms are shown in table VIII. The Fe-O distances are between 1.63 and 2.45Å, and the O-O dis-

Surface Structures of α-Fe2O3(0001) Phases determined by LEED Crystallography, G. Ketteler et al., Surf. Rev. Lett. 8 (2001), 661.

8

tances are between 2.55 and 3.29Å. The optimized Debye temperatures are 350K for Fe and 450 K for O. The opti- mized imaginary part of the inner potential is −7 eV and the real part is 9.0 eV.

Table VII: Atomic coordinates (in Å) for the α-Fe$_2$O$_3$(0001) bulk structure and for the surface structure model which gives the best fit between experimental and theoretical I-V curves for the film forming in 1 mbar O$_2$ (R$_P$=0.381).

Layer	Atom	surface structure (optimized)			bulk structure (crystal structure)		
		z	x	y	z	x	y
1	O	-0.708	-0.133	-1.574	-0.846	-0.145	-1.762
1	O	-0.708	-1.280	0.902	-0.846	-1.454	1.007
1	O	-0.708	1.521	0.657	-0.846	1.599	0.755
2	Fe	-0.253	0.000	0.000	0.000	0.000	0.000
3	Fe	0.608	-1.454	-2.518	0.5945	-1.454	-2.518
4	O	1.450	-1.245	-0.787	1.441	-1.308	-0.755
4	O	1.450	-0.062	1.471	1.441	0.000	1.511
4	O	1.450	1.306	-0.669	1.441	1.308	-0.755
5	Fe	2.345	1.454	2.518	2.287	1.454	2.518
6	Fe	3.007	0.000	0.000	2.881	0.000	0.000

Table VIII: Atomic coordinates (in Å) for the α-Fe$_2$O$_3$(0001) bulk structure and for the surface structure model which gives the second best fit between experimental and theoretical I-V curves for the film forming in 1 mbar O$_2$ (R$_P$=0.408).

Layer	Atom	surface structure (optimized)			bulk structure (crystal structure)		
		z	x	y	z	x	y
1	O	-0.709	-0.235	-1.723	-0.846	-0.145	-1.762
1	O	-0.709	-1.370	1.074	-0.846	-1.454	1.007
1	O	-0.709	1.615	0.650	-0.846	1.599	0.755
2	Fe	0.130	0.000	0.000	0.000	0.000	0.000
3	Fe	0.157	-1.454	-2.518	0.5945	-1.454	-2.518
4	O	1.507	-1.731	-0.773	1.441	-1.308	-0.755
4	O	1.507	0.209	1.878	1.441	0.000	1.511
4	O	1.507	1.522	-1.122	1.441	1.308	-0.755
5	Fe	2.337	1.454	2.518	2.287	1.454	2.518
6	Fe	3.001	0.000	0.000	2.881	0.000	0.000

Surface Structures of α-Fe2O3(0001) Phases determined by LEED Crystallography, G. Ketteler et al., Surf. Rev. Lett. 8 (2001), 661.
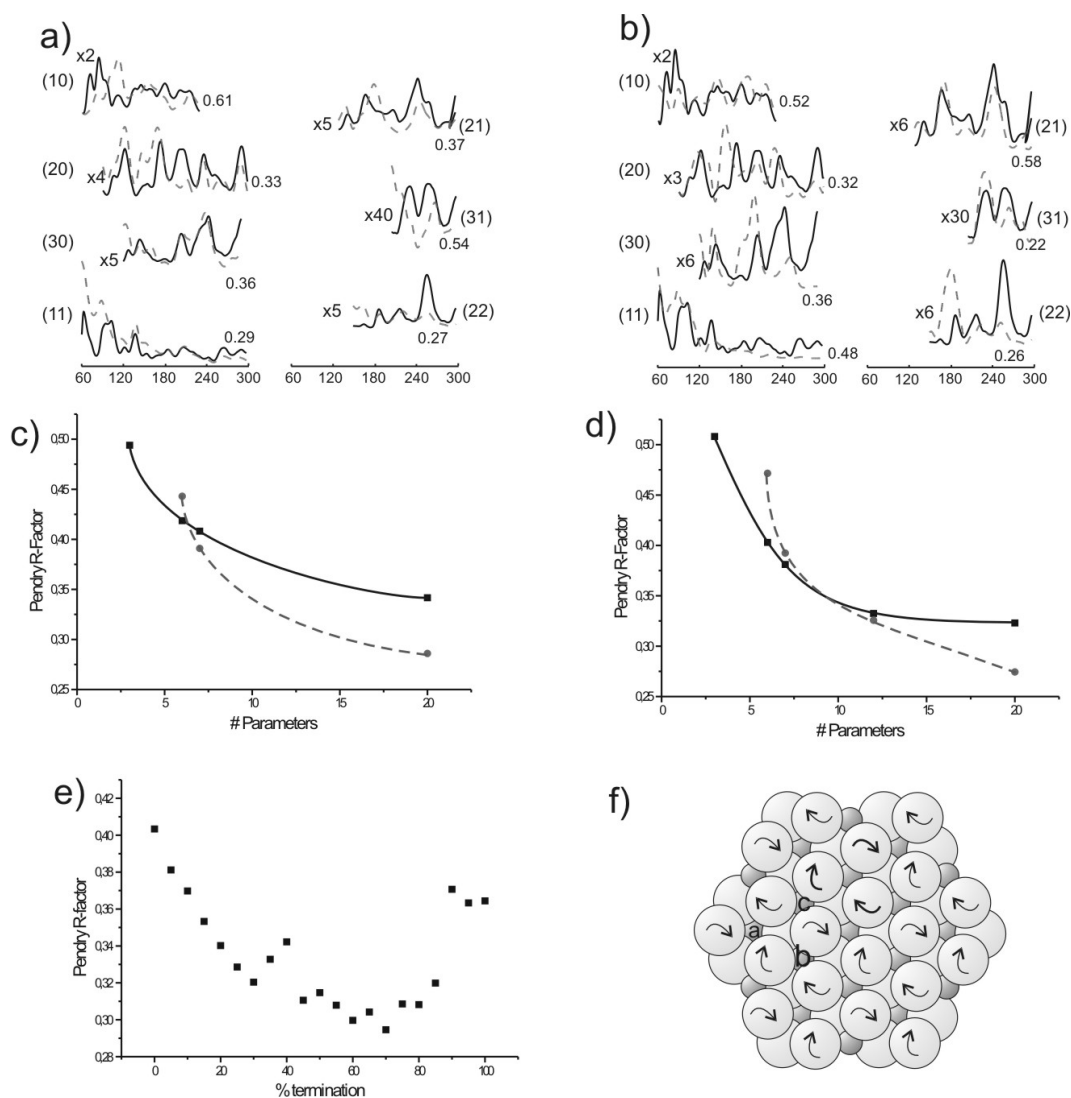
9

Fig. 4: (a) Experimental (solid lines) and theoretical (dashed lines) LEED I-V spectra of the best fit surface structure for the α-Fe$_2$O$_3$(0001) film prepared in 1 mbar O$_2$. (b) Experimental (solid lines) and theoretical (dashed lines) LEED I-V spectra of the second best fit surface structure for the α-Fe$_2$O$_3$(0001) film prepared in 1 mbar O$_2$. The Pendry R factors for the single beams are also indicated. (c), (d) Decrease of the Pendry R factor in dependence of the atomic parameters allowed to relax (solid curves) compared to the minimum values expected for a physically meaningful improvement (dashed curves). For details see text. (e) Improvement of the Pendry R factor for a film prepared in 1 mbar O$_2$ by mixing the best and second-best fit structure models. (f) Schematic top view showing the rotation of oxygen trimers in the first layer of the second-best fit structure model.

Table IX: Comparison of experimental and theoretical interlayer relaxations of iron and oxygen terminated surfaces of α-Fe$_2$O$_3$(0001), α-Al$_2$O$_3$(0001), and α-Cr$_2$O$_3$(0001). Our results are indicated in table II.

1. O-terminated structure determinations:

| | α-Al$_2$O$_3$(0001) | α-Fe$_2$O$_3$(0001) | α-Al$_2$O$_3$(0001) | **Our results** | | |
| | DFT, (Ref. 60) | DFT, (Ref. 13) | LEED, (Ref. 61) | 10^{-5} mbar O$_2$ | 1 mbar O$_2$ | |
				model #2	model #1	model #2
Δ_{12}	-15%	-1%	+3%	+10%	-54%	-1%
Δ_{23}	+7%	-79%	-2%	+28%	+46%	-95%
Δ_{34}	+12%	+37%	+12%	-24%	-1%	+35%

2. Metal-terminated structure determinations:

| | α-Al$_2$O$_3$(0001) | α-Al$_2$O$_3$(0001) | α-Al$_2$O$_3$(0001) | α-Cr$_2$O$_3$(0001) | **Our results** |
| | DFT, (Ref. 62) | DFT, (Ref. 63) | DFT, (Ref. 60) | LEED, (Ref. 64) | 10^{-5} mbar O$_2$ |
					model #1

Δ_{12}	-87%	-86%	-77%	-60%	-79%
Δ_{23}	+3%	+3%	+11%	-3%	+4%
Δ_{34}	-42%	-54%	-34%	-21%	+35%

α-Fe2O3(0001) DFT, (Ref. 13)	α-Al2O3(0001) CTRD, (Ref. 65)	α-Cr2O3(0001) HF, (Ref. 66)	α-Fe2O3(0001) Ewald method, (Ref. 67)	α-Fe2O3(0001) XPD, (Ref. 52)
Δ_{12}　　-57%	-51%	-50%	-49%	-41%
Δ_{23}　　+7%	+16%	+3%	-3%	+18%
Δ_{34}　　-33%	-29%	0%	-41%	-8%

α-Al2O3(0001) LEED, (Ref. 61)
Δ_{12}　　+29%
Δ_{23}　　-5%
Δ_{34}　　+57%

4. Discussion

4.1. High pressure surface structure

In 1 mbar O_2, two structure models with the same layer sequence but different interlayer relaxations give similar Pendry R-factors which both being unsatisfactorily high. We tried to improve the fit by mixing both models and indeed, the R-factor decreases to 0.29 for a mixture of ~40:60 (see fig. 4(e)). We have no explanation why such a mixture should be formed, nevertheless, the improvement is significant. No evidence for such a mixture is found in other experiments but this might also be due to very similar chemical and electronic surface properties of both structure. Oxygen layers in both structures are nearly at the same positions (compare z coordinates in tables 7 and 8) while only position of the iron layers inbetween differ strongly. Table IX compares both structures with theoretical and experimental results. In general, experimental and theoretical investigations of the surface structure of corundum-type metal oxides deviate significantly from one to the other. No general trend can be observed and even the direction of the relaxation (contraction vs. expansion) differs strongly. Our second best structural model agrees very well with the structural model found by Wang et al. in ab-initio DFT calculations.[13] Even there a rotation of oxygen trimers in the first layer by 10° was observed. The same unusual kind of reconstruction was observed in our analysis where a similar rotation of 3° was found.

On the basis of this LEED analysis, we can conclude that the surface structure forming in 1 mbar oxygen pressure is oxygen terminated, although we could not determine whether one of the two structural models or a mixture of both represents the ´true´ surface structure. Although the atomic parameters of the second best structure model match very well with those determined by Wang et al., we find no experimental evidence for this structure since both iron atoms underneath the oxygen layer are in the same layer and one would expect that changes in the local density of states in the proximity of the additional iron atoms should be imaged in STM which was not the case. As will be shown below, also the good agreement between experimental I-V spectra from films prepared in 10^{-1} to 10^{-4} mbar O_2 with theoretical I-V spectra from a mixture of the best fit model with the best fit 'low-pressure' model (see fig. 9) favours the best fit model over the second best one. How-

ever, a mixture of both models decreases the R-factor considerably to 0.29 and thus may have formed in the high oxygen pressure environment.

A pure oxygen termination is polar and should not be stable according to electrostatic considerations.[14] The bonds of compound surfaces possess a large covalent contribution and a purely ionic description is not sufficient. Especially in the surface region, the ionicity of the atoms can be strongly reduced as has been shown by a Mulliken population analysis of $V_2O_5(010)$.[37] Strong relaxations lead to a stronger overlap of the ionic radii and the covalent contribution is increased thus reducing the dipole moment. Even though large relaxations may reduce the dipole moment at the surface, an oxygen termination is still polar and should not be stable. Nevertheless, films (in contrast to semi infinite materials) possess two interfaces, one to the gas phase and one to the substrate. Intuitively, the interface to the gas phase with its dangling bonds should be much more sensitive to alterations of environmental variables while the interface is supposed to be more resistive due to the spatial isolation from the gas environment and due to the covalent (or ionic) bonding to the substrate. Thus, we suppose that the most stable configuration of films on chemically inert substrates consists of charge compensated repeat units starting from the interface to the substrate. This has recently been emphasized by C. Noguera who stressed that the boundary conditions at the interface may also be of prime inportance for the stability of thin polar oxide films[19] as shown schematically for the α-Fe2O3(0001) surface in fig. 5. In case the substrate is bound via an iron layer to the substrate (shown schematically in fig. 5(a) and (b)) any termination may be stabilized since no *macroscopic* dipole moment exists, and specifically an oxygen termination is associated with a *surface* dipole moment which may easily be reduced by large relaxations as observed in our LEED analysis. We know from high resolution transmission electron microscopy and photoelectron diffraction measurements that the precursor FeO(111) and Fe3O4(111) films are bound via an iron layer to the metal substrate[38,39] and the same is expected for α-Fe2O3(0001) so that we suppose that this film is stabilized in this way in combination with the strong relaxations observed in this study.
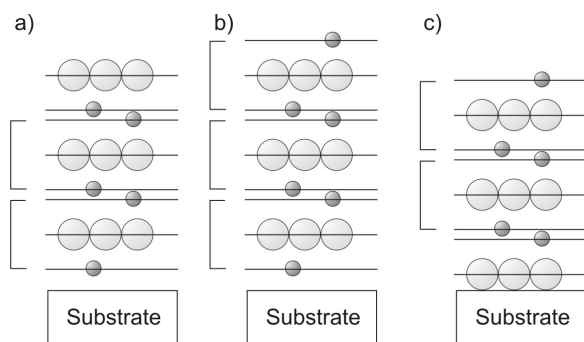
Fig. 5: Schematic side views of α-Fe$_2$O$_3$(0001) films grown on a substrate with different layer configurations. The brackets denote charge compensated repeat units. Note the absence of a macroscopic dipole moment in the shown configurations. (Figure modified after Ref. 19).

In contrast, Chambers et al. always obtained a strongly relaxed iron terminated α-Fe$_2$O$_3$(0001) film on α-Al$_2$O$_3$(0001) substrates, even under heavily oxidizing conditions, and they concluded that only this autocompensated surface is stable.[15] In general, it is difficult to compare films grown by molecular beam epitaxy (MBE) with thermally grown films which can be prepared at real thermodynamic equilibrium. Even if both preparation conditions are able to generate films in equilibrium with an oxygen environment, it is difficult to compare the oxygen plasma generating a chamber pressure of 2×10^{-5} Torr with an oxygen pressure, and it is not assured that this plasma is as oxidizing as 1 mbar molecular O$_2$ at 1100K to produce an oxygen terminated surface. But even if this is the case, we want to stress that the differently terminated films may originate from the different substrates used: From the autocompensation principle, α-Fe$_2$O$_3$(0001) single crystals should only be stable with an iron termination. The same situation occurs when growing hematite films on isostructural substrates like α-Al$_2$O$_3$(0001)single crystals, since these substrates have the same stacking sequence and similar layer distances. In contrat, on inert metal substrates, as pointed out above, an oxygen termination may well be stable in case the stacking sequence of the hematite film starts with a single iron layer as expected for the heteroepitaxially grown films in this study.

4.2. Low pressure surface structures

The LEED analysis of α-Fe$_2$O$_3$(0001) films annealed in 10^{-5} mbar O$_2$ identified three completely different structural models to have similar and quite good Pendry R-factors. All other relaxed or terminated structures turned out to give significantly worse results. All three models show a poor agreement for the (11) beam, and the O-O distances are in some cases very short leading to an overlap of the ionic radii of oxygen for all three models. It was not possible to identify unambiguously one structural model. Several reasons may be responsible: Statistically distributed adsorbates can be seen after a while in STM,[12] this contamination should proceed even faster below the condensation temperature of water where the I-V curves were recorded.[4] These adsorbates and/or some structural disorder may be responsible for the increased background intensity in the LEED images. Above 300eV, the peak to noise ratio is very low, therefore the total energy range is restricted to about 1300eV. An unambiguous identification of one structural model would require a larger energy range which we were not able to produce for the investigated preparation conditions. Nevertheless, information from other surface sensitive techniques helps to identify the most likely structural model.

The iron and oxygen terminated models were compared with results from theoretical and experimental structure determinations in table IX. Almost all theoretical and experimental determinations reveal large interlayer relaxations for the first interlayer distances. For metal terminated surfaces these are tremendous and the first two interlayer distances agree reasonably with the iron terminated structure model from our LEED analysis. The values for oxygen terminated structures scatter strongly, even an expansion of the first interlayer distance is described in the literature. Such an expansion would even increase the dipole moment of the polar oxygen termination and thus makes physically no sense.

To distinguish between the oxygen (best fit) and iron (second best fit) terminated structure models, we performed ion scattering spectroscopy (ISS) measurements which will be published elsewhere.[40] These measurements indicate that a signal from Fe cold only be observed for incidence angles below 45° with respect to the surface normal. For higher incidence angles (grazing incidence), no iron signal could be detected. This proves that the surface of α-Fe$_2$O$_3$(0001) films annealed in 10^{-5} mbar O$_2$ is oxygen terminated.

One possible explanation for the outward relaxation of the first layer spacing is a hydroxilation of the surface as proposed by Wang et al. for α-Al$_2$O$_3$(0001).[41] The surface structure of Fe$_3$O$_4$(111) was found to be terminated by ¼ ML iron.[42] This surface structure is fairly open and exposes acidic as well as basic sites and was found to be very reactive against dissociative water adsorption.[43,44] Iron terminated α-Fe$_2$O$_3$(0001) would expose $^1/_3$ ML iron and should be even more reactive against hydroxilation since no oxidation is necessary to form one of the stable iron hydroxides. Indeed, the isostructural α-Al$_2$O$_3$(0001), α-Cr$_2$O$_3$(0001) and α-Fe$_2$O$_3$(0001) surfaces have been found to get hydroxilated in water environment.[41,45-47] Time-of-flight scattering and recoiling spectrometry always detected hydrogen within a few minutes on α-Al$_2$O$_3$(0001) surfaces, even after several anneals to 1100°C in vacuum although the origin of these hydrogen species were supposed not to come from the residual gas.[48] For the clean α-Al$_2$O$_3$(0001) surface an aluminium terminated surface was predicted to be stable even under high oxygen partial pressures.[41] However, if hydrogen or water species are present on the surface, an oxygen terminated surface becomes more stable. Hydroxilation of α-Al$_2$O$_3$(0001) was also verified experimentally by crystal truncation rod diffraction.[45] The mechanism of hydroxilation by water was predicted to proceed preferentially via a dissociative 1-4 adsorption geometry on the aluminium terminated surface catalyzed by a second water molecule.[49,50] Also for the oxygen terminated (0001) surface of α-Al$_2$O$_3$ a hydroxilation was predicted which stabilizes the surface especially in case many oxygen vacancies are present (or created) at the surface.[51]

For α-Fe$_2$O$_3$(0001), hydroxilation was found to be even more facile than on α-Al$_2$O$_3$(0001).[45,52] For an iron terminated and even more for an oxygen terminated α-Fe$_2$O$_3$(0001) surface, the hydroxilation energy was calculated to be very large (-298.1kJ/mol).[53] An iron terminated surface was found to be completely unstable in presence of excess water (>67% coverage) and was predicted to relax, leaving an oxygen terminated hydrated layer with Fe(OH)$_3$ subunits behind.[54] Hydroxyl species on the (0001) face of hematite were found to be difficult to remove (in contrast to surface OH groups on other hematite planes) and were thermally stable up to at least 1073K in oxygen atmosphere as evidenced by infrared spectroscopy,[55] and hydroxyl on iron terminated α-Fe$_2$O$_3$(0001) could not be removed by excessive heating at 900K without reducing the near-surface region to Fe(II).[52] Recently we performed com-

Surface Structures of α-Fe2O3(0001) Phases determined by LEED Crystallography, G. Ketteler et al., Surf. Rev. Lett. 8 (2001), 661.

12

bined LEED and thermal desorption spectroscopy measurements showing that α-Fe$_2$O$_3$(0001) films annealed in 10^{-5} mbar oxygen decompose in vacuum above 900K and besides O$^+$ and Fe^{++} large amounts of H$_2$O$^+$ and OH$^+$ were detected simultaneously. This shows that if hydroxyl groups are formed on this surface, these are very stable and could not be removed without decomposition of the film. Since the reaction of oxygen with hydrogen to form water is exothermic and thus not favoured at high temperatures, the immediate reaction of the liberated oxygen with residual gas hydrogen to form the species observed in the TD spectra is unlikely.

Thus, we would expect that both the oxygen and iron terminated surface α-Fe$_2$O$_3$(0001) films should get hydroxilated in excess water and that once hydroxilated these surfaces are very stable. A comparison of the relaxations of hydroxilated surfaces reveals an oxygen termination with an expansion of the first interlayer distance of +3 to +20% (see table X) which is of the same order than the outward relaxation of our best fit structure forming in 10^{-5} mbar thus suggesting that this surface is hydroxilated. Due to their low scattering intensity, hydrogen atoms in form of an OH or H-termination cannot be detected by LEED.

Table X: Comparison of the expansion of the first interlayer distance of proposed hydroxy terminated α-Fe$_2$O$_3$(0001) and α-Al$_2$O$_3$(0001) surfaces from theoretical and experimental investigations.

	α-Al$_2$O$_3$(0001) DFT, (Ref. 41)	α-Al$_2$O$_3$(0001) atomistic potential (Ref. 51)	α-Al$_2$O$_3$(0001) CTRD, (Ref. 45)	α-Al$_2$O$_3$(0001) LEED, (Ref. 61)	α-Fe$_2$O$_3$(0001) atomistic potential (Ref. 54)	**Our result 10^{-5} mbar O$_2$ model #1**
Δ_{12}	+3%	+7%	+20%	+14%	<3%	+10%

The residual gas in an UHV chamber may well hydroxilate oxidic compounds as we have also observed for potassium iron oxides.[56] The time between final anneal and start of the LEED measurement at 120K or STM measurements was at least about 30 minutes. During this time, the surface was exposed to the residual gas in the ultra-high vacuum chamber and in the preparation chamber (base pressure 5×10^{-8} mbar). The water partial pressure in this chamber may be quite high when oxygen is let into this chamber.

If a hydroxilation of the surface occured by cooling to 120K (where even α-FeOOH may become thermodynamically more stable)[57], the I-V characteristic at room temperature should look different. Therefore we recorded I-V spectra from a film annealed in 10^{-5} mbar O$_2$ at room temperature. In general, the I-V characteristics resemble each other: The peak positions are almost the same while the peak intensities have changed. In general, the background is higher and the intensity is reduced, therefore the information which can be gathered from these curves is less than from I-V spectra recorded at 120K. Nevertheless, in this case the Pendry R-factor of the oxygen-terminated model increases slightly to 0.254 while the agreement for the iron terminated model is 0.258 and thus almost identical to I-V curves recorded at 120K. Still, these two models yield the best agreement between experiment and theory. The close similarity of spectra taken at 120K and 298K implies that if a hydroxilation of the surface occurs, this happens already at room temperature and may only be enhanced at the temperature of liquid nitrogen since hydroxilation is thermodynamically favored with decreasing temperature. The first part to get hydroxilated is the surface and thus partial hydroxilation of the surface is very likely at room temperature. However, a quantum-chemical investigation of the surface energies would be necessary to determine the stability and extent of surface hydroxilation quantitatively. A fully hydroxilated termination would possess a stoichiometry of Fe(OH)$_3$ in the topmost surface region as predicted by Jones et al.[54], but partial hydroxilation resulting in a α-FeOOH surface region is also possible.

Atomically resolved STM images of the presented α-Fe$_2$O$_3$(0001) films for oxygen annealing pressures >10^{-5} mbar reveal two different domains which are separated by steps with an apparent height difference of about 1.5Å[12] (fig. 6). These domains exhibit different atomic corrugation amplitudes of 0.3 and 0.1 Å, respectively. The interpretation that these domains are oxygen and iron terminated as suggested by the DFT calculations of Wang et al.[13] conflict with the protrusions of both terminations being in registry. This might only be true in case the local density of states at the Fermi level in one of both terminations possesses a maximum electron density shifted to a hollow site and not above the iron atoms which is unlikely. The partial density of states of oxygen as well as iron terminated α-Fe$_2$O$_3$(0001) surface was calculated to be dominated by the Fe-d orbitals,[58] therefore the protrusions in the STM images were assigned to iron atoms in the top or even the second layer (as also suggested by Eggleston).[59] Nevertheless, the protrusions of both domains can not be in registry for a mixture of bulk truncated iron and oxygen terminated domains whereas protrusions of a coexisting oxygen and hydroxy termination would indeed be in registry. A registry shift of iron atoms in the topmost layer of an iron termination can be ruled out by the presented LEED analysis. Films prepared in 10^{-5} mbar and 1 mbar O$_2$ possess a different local density of states (LDOS) as indicated by the different corrugation amplitudes. In case our interpretation is correct, the LDOS of the iron layer below the oxygen layer is different from the LDOS of an iron layer below the hydroxy termination leading to apparant step heights of 1-1.5Å instead of the determined geometric distance between the oxygen planes of ~0.5Å.
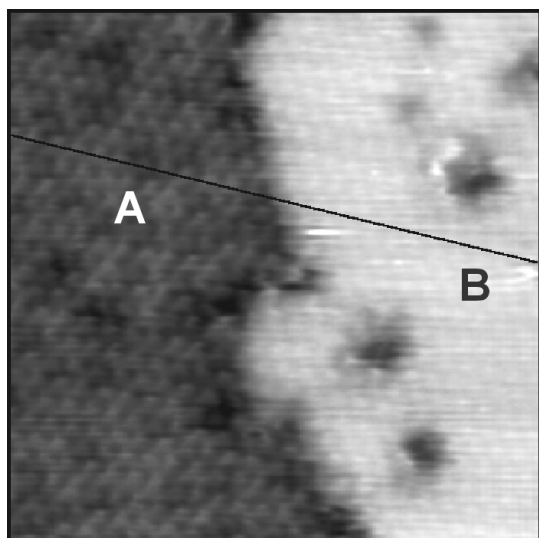
Surface Structures of α-Fe2O3(0001) Phases determined by LEED Crystallography, G. Ketteler et al., Surf. Rev. Lett. 8 (2001), 661.

13

Fig. 6: $120 \times 120 \text{Å}^2$ atomic resolution STM image of α-$Fe_2O_3(0001)$ annealed in 10^{-1} mbar O_2. (V_B=+1.3V, I_t=1.25nA). Two domains are separated by a height distance of 1.5Å. Note that the protrusions of both domains exhibit different corrugation amplitudes and that they are in registry. From Ref 12.

To summarize, all presented results are consistent assuming that in 10^{-5} mbar a hydroxyl terminated surface structure (model #1 from section 3C) is formed while in 1 mbar the surface is oxygen terminated (see section 3D). These two terminations could be analyzed by the modified Tensor LEED program to model mixed terminated domains as observed in STM for annealing pressures between 10^{-5} and 1 mbar. Fig. 7 shows the improvement of the Pendry R-factor for a film prepared in 1mbar (a), 10^{-1} mbar (b), 10^{-4} mbar (c) and 10^{-5} mbar (d) O_2 by mixing the best fit structure models of the nearly single terminated films. The calculations reveal that the admixture of the high pressure model for the experimental data recorded from a film prepared in 10^{-5} mbar O_2 gives no improvement (fig. 7(d)). A minimum Pendry R-factor is obtained for relative surface areas of about 20% "1mbar-structure" for a film prepared

in 10^{-4} mbar (fig. 7(c)) and of about 50-55% in 10^{-1} mbar O_2 (fig. 7(b)). The modelling of the film prepared in 1 mbar O_2 may even be slightly improved when admixing about 5-10% of the best fit "10^{-5} mbar-structure". These results reflect approximately the relative amounts of both domains as estimated from STM large scale images[12] and supports that both domains can be correlated with the identified best fit structures forming in 10^{-5} and 1 mbar O_2. Mixing the other 'low-pressure' models does not reflect the general trend observed in STM and especially the iron terminated model identified in 10^{-5} mbar oxygen with the second best R-factor gives significantly worse improvements (Hamilton ratio H < 2.6) upon mixing. Mixing the second best 'high-pressure' model with the best fit 'low-pressure model' also leads to a significant improvement of the R-factor, nevertheless, this does not reflect the general trend observed in STM and especially for films prepared in 1mbar and 10^{-5} mbar oxygen unrealistic percentages were obtained. Thus we propose that even if in 1mbar oxygen a mixture of both models is formed, annealing at intermediate oxygen pressures leads to the selective hydroxilation of the domains with the second best 'high-pressure' model.

We cannot say whether hydroxilation of an initially iron or oxygen terminated surface produces the hydroxyl termination, since hydroxilation of an iron termination or of a defective oxygen termination both are predicted to proceed fast.[51,54] It is reasonable to assume that after annealing in lower oxygen pressures an iron termination or defective oxygen termination is initially formed which is quickly hydroxilated at room temperature while after annealing in high oxygen pressures a less defective and therefore more inert oxygen termination is formed. If indeed a mixture of both 'high-pressure' models coexists than the second best fit structure is more reactive in this respect and gets hydroxilated first. Thus, it seems that α-$Fe_2O_3(0001)$ undergoes a surface phase transition, specifically a hydroxilation, after annealing in 10^{-5} or 1 mbar O_2. Thermodynamics excludes two coexisting domains, so that kinetic reasons are responsible for the observed mixed terminated domains (see Ref. 4).
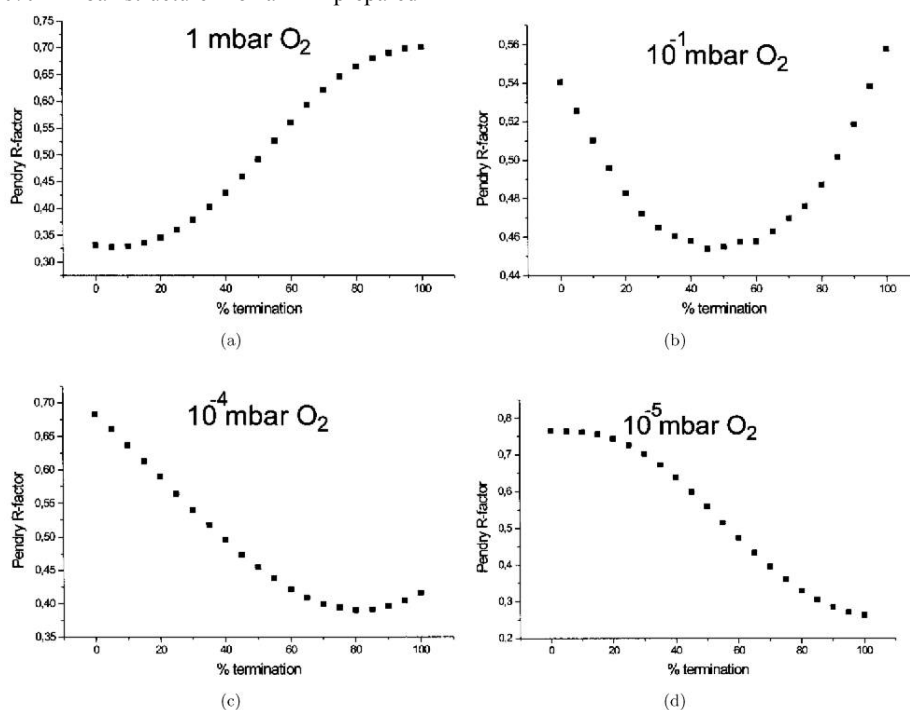

(a)

(b)

(c)

(d)

Fig. 7: Improvement of the Pendry R-factor for a film prepared in 1 mbar O_2 (a), 10^{-1} mbar O_2 (b) and 10^{-4} mbar O_2 (c) and 10^{-5} mbar O_2 (d) by mixing the best fit structure models of the nearly single terminated films prepared in 1 mbar O_2 and 10^{-5} mbar O_2.

Surface Structures of α-Fe2O3(0001) Phases determined by LEED Crystallography, G. Ketteler et al., Surf. Rev. Lett. 8 (2001), 661.

14

We suggest the following model for the formation of both surface phases (fig. 8): In order to transform $Fe_3O_4(111)$ films into α-Fe_2O_3(0001) within reasonable time, we initially oxidized in oxygen pressures $>10^{-3}$ mbar. This leads to an oxygen termination of the (0001) plane which may have vacancies. Annealing at different pressures now adjusts different adsorption-desorption equilibria. For high pressures, oxygen vacancies are rare and an inert oxygen layer terminates the film. With decreasing oxygen pressure, the adsorption-desorption equilibrium establishes more and more oxygen vacancies by desorption of oxygen from the terminating layer which are the initial starting point for the hydroxilation. In 10^{-1} mbar O_2, only a few vacancies may be created while for lower pressures, more statistically distributed starting points for hydroxilation are formed.

This explains why the lateral domain extension decreases with decreasing oxygen pressure as observed in STM (from 900Å at 10^{-1} mbar to 30 Å at 10^{-4} mbar O_2).[12] In 10^{-5} mbar O_2 either an iron termination or an oxygen termination with many vacancies may be formed which both will be hydroxilated quickly. We assume that this hydroxilation even occurs in residual gas pressures of 5×10^{-8} mbar within the time necessary to transfer the samples from the preparation cell to the STM or to cool the sample to 120K (which both take at least 30 minutes). Additionally, the water partial pressure in the high pressure cell is significantly increased during high pressure oxidations due to the reaction of the oxygen molecules with adsorbed hydrogen on the chamber walls.
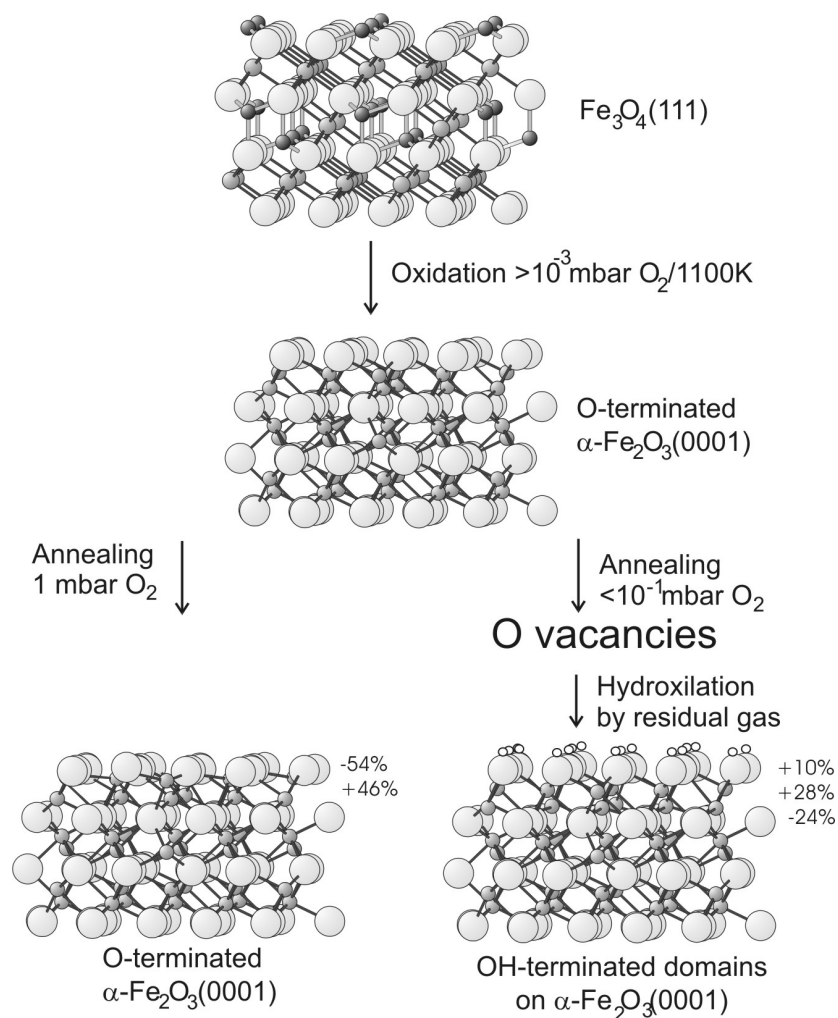

Fig. 8: Proposed mechanism for the hydroxilation of an oxygen terminated α-Fe_2O_3(0001) film after annealing in low oxygen pressures. Vacancies are created in oxygen pressures below 1 mbar which are quickly hydroxilated by the residual gas.

For intermediate pressures, the adsorption-desorption equilibirium creates less vacancies which then are hydroxilated, therefore the hydroxilation of these films is slower and leads to less hydroxilated surface domains. The hydroxilated surface seems to be very stable even at high temperatures. We propose that this is due to the expected stability for such a charge compensated surface termination. We want to stress that there might exist experimental conditions which may result in iron terminated α-Fe_2O_3(0001) as predicted by Wang et al.,[13] since we ascribe the observed hydroxilation to a vacancy based mechanism starting from the oxygen termination. Hydroxilation may be kinetically favoured over a reconstruction of the surface into an iron termination which would involve a more severe reorganization of the surface. The relative surface free energies of

hydroxilated and non-hydroxilated (0001) planes of α-Fe_2O_3 have not yet been treated theoretically, such calculations may verify the high stability suggested by our results.

5. Summary
We presented an extensive Tensor LEED analysis of the surface structure of α-Fe_2O_3(0001) films prepared in oxygen pressures between 1 and 10^{-5} mbar. Due to the high complexity of this system we were not able to get non-ambiguous results. Nevertheless, this structural analysis gives valuable information on the surface structure on a qualitative level and in combination with results from other surface sensitive methods we were able to deduce the most likely surface structures.

Surface Structures of α-Fe2O3(0001) Phases determined by LEED Crystallography, G. Ketteler et al., Surf. Rev. Lett. 8 (2001), 661.

15

Epitaxial α-Fe_2O_3(0001) films are prepared by high pressure oxidation of Fe_3O_4(111) around 1100K in oxygen pressures $>10^{-3}$ mbar O_2. Dynamical LEED calculations in combination with ion scattering spectroscopy and scanning tunneling microscopy are only consistent with an oxygen terminated surface structure after annealing in 1 mbar O_2 while annealing in 10^{-5} mbar O_2 results in a hydroxy termination. The surface structure forming in 1 mbar O_2 is oxygen terminated. Since this film is bound via an iron layer to the Pt(111) substrate, this surface is associated with a surface dipole moment which no longer is infinite and which can be compensated by the large relaxations observed for the first two layer distances. We propose a model where subsequent annealing of the oxygen terminated film in oxygen pressures between 10^{-1} to 10^{-5} mbar O_2 establishes oxygen vacancies. These oxygen vacancies are the starting point for a fast hydroxilation of the surface by residual gas water.

We show that the surface termination of α-Fe_2O_3(0001) is highly dependent on the ambient conditions and using significantly different substrates (e.g. oxidic substrates) or preparation conditions like for instance molecular beam epitaxy may lead to completely different surface structures. The boundary conditions at the interface with the substrate and not only the surface terminations are of major importance for the stabilization of thin, epitaxial polar oxide films.

Acknowledgements

References

[1]   D. W. Goodman. Surf. Sci. **299/300**, 837 (1994).
[2]   J. H. Larsen, Ib Chorkendorff, Surf. Sci. Rep. **35**, 163 (1999).
[3]   A. Muan, Am. J. Sci. **256**, 176 (1958).
[4]   G. Ketteler, W. Weiss, W. Ranke, R. Schlögl, Phys. Chem. Chem. Phys. **3**, 1114 (2001).
[5]   W. Weiss, R. Schlögl, Top. Catal. **13**, 75 (2000).
[6]   E.H. Lee; Calal. Rev. **8,** 285 (1973).
[7]   J. W. Geus, Appl. Catal. **25**, 313 (1986).
[8]   M. Muhler, R. Schlögl and G. Ertl; J. Catal. **138**, 413 (1992).
[9]   C. Kuhrs, Y. Arita, W. Weiss, W. Ranke, and R. Schlögl; Top. Catal. **14**, 111 (2001).
[10]   W. Weiss, Surf. Sci. **377-379**, 943 (1997).
[11]   Sh. K. Shaikhutdinov, Y. Joseph, C. Kuhrs, W. Ranke, W. Weiss, Farad. Discuss. **114**, 363 (1999).
[12]   Sh. K. Shaikhutdinov, W. Weiss, Surf. Sci. **432**, L627 (1999).
[13]   X.-G- Wang, W. Weiss, Sh. K. Shaikhutdinov, M. Ritter, M. Petersen, F. Wagner, R. Schlögl, M. Scheffler, Phys. Rev. Lett. **81**, 1038 (1998).
[14]   P. W. Tasker, J. Phys. C: Sol. State Phys. **12**, 4977 (1979).
[15]   S. A. Chambers, S. I. Yi, Surf. Sci. **439**, L785 (1999).
[16]   C. Noguera, *Physics and Chemistry at Oxide surfaces*, Cambridge University Press 1996.
[17]   V. E. Henrich, P. A. Cox, *The surface science of metal Oxides*, Cambridge University Press 1994.
[18]   H.-J. Freund, Angew. Chem. **109**, 444 (1997).
[19]   C. Noguera, J. Phys.: Condens. Matter **12**, R367 (2000).
[20]   A. Barbier, C. Mocuta, H. Kuhlenbeck, K. F. Peters, B. Richter, G. Renaud; Phys. Rev. Lett. **84**, 2897 (2000).
[21]   W. Weiss, M. Ritter, D. Zscherpel, M- Swoboda, R. Schlögl, J. Vac. Sci. Technol. **A16**, 21 (1998).
[22]   W. Weiss and M. Ritter; Phys. Rev. **B59,** 5201 (1999).
[23]   N. G. Condon, F. M. Leibsle, A. R. Lennie, P. W. Murray, D. J. Vaughan, G. Thornton, Phys. Rev. Lett. **75**, 1961 (1995).
[24]   A. Barbieri, M.A. Van Hove, *Symmetrized Automated Tensor LEED Package*, available from M. A. Van Hove, Lawrence Berkeley Laboratory, 94720 Berkeley, CA, USA.
[25]   P. J. Rous, J. B. Pendry, D. K. Saldin, K. Heinz, K. Müller, N. Bickel, Phys. Rev. Lett. **57**, 2951 (1986).
[26]   P.J. Rous and J.B. Pendry; Comput. Phys. Commun. **54,** 137, 157 (1989), Surf. Sci. **219**, 355 (1989).
[27]   J. B. Pendry, J. Phys. C: Solid State Phys. **13**, 937 (1980).
[28]   A. Barbieri, W. Weiss, M. A. Van Hove, G. A. Somorjai, Surf. Sci. **302**, 259 (1994).
[29]   W. C. Hamilton, Acta Cryst. **18**, 502 (1965).
[30]   E. Prince, *Mathematical Techniques in Crystallography and Materials Science*, Springer-Verlag New York 1982.
[31]   C. F. Walters, K. F. McCarty, E. A. Soares, M. A. Van Hove, Surf. Sci. Lett. **464**, L732 (2000).
[32]   R. W. G. Wyckoff, *Crystal Structures*, 2nd ed., Vol. I-III, Interscience Publishers 1982.
[33]   M. Ritter; PhD thesis, TU Berlin (1998).
[34]   M.A. Van Hove, W.H. Weinberg, C.-M. Chan; *Low Energy Electron Diffraction*, Springer-Verlag, Berlin Heidelberg (1986)
[35]   T. Gloege, H. L. Meyerheim, W. Moritz, D. Wolf, Surf. Sci. Lett. **441**, L917 (1999).
[36]   J. Ahdjoudj, C. Martinsky, C. Minot, M. A. Van Hove, G. A. Somorjai, Surf. Sci. **443**, 133 (1999).
[37]   K. Hermann, M. Witko, R. Druzinic; Farad. Discuss. **114**, 53 (1999).
[38]   V. V. Roddatis, D. Su, C. Kuhrs, W. Ranke, R. Schlögl; Thin Solid Films, (2001), accepted.
[39]   Y.J. Kim, C. Westphal, R. X. Ynzunza, H. C. Galloway, M. Salmeron, M. A. Van Hove, C. S. Fadley; Phys. Rev. **B55**, R13448 (1997).
[40]   D. Frickel, Y. Arita, W. Ranke; in preparation.
[41]   X.-G. Wang, A. Chaka, M. Scheffler; Phys. Rev. Lett. **84**, 3650 (2000).
[42]   M. Ritter and W. Weiss; Surface Science **432**, 81 (1999).
[43]   Y. Joseph, C. Kuhrs, W. Ranke, M. Ritter, W. Weiss, Chem. Phys. Lett. **314**, 195 (1999).
[44]   Y. Joseph, W. Ranke and W. Weiss, J. Phys. Chem B **104**, 3224 (2000).
[45]   P. J. Eng, T. P. Trainor, G. E. Brown Jr., G. A. Waychunas, M. Newville, S. R. Sutton, M. L. Rivers; Science **288**, 1029 (2000).
[46]   P. Liu, T. Kendelewicz, G.E. Brown, E.J. Nelson, and S.A. Chambers, Surf. Sci. **417**, 53 (1998).
[47]   M. A. Henderson, S. A. Chambers; Surf. Sci. **449**, 135 (2000).
[48]   J. Ahn, J. W. Rabelais; Surf. Sci. **388**, 121 (1997).
[49]   J. M. Wittbrodt, W. L. Hase, H. B. Schlegel; J. Phys. Chem. **102**, 6539 (1998).
[50]   K. C. Hass, W. F. Schneider, A. Curioni, W. Andreoni; Science **282**, 265 (1998).
[51]   M. A. Nygren, D. H. Gay, R. A. Catlow; Surf. Sci. **380**, 113 (1997).

Surface Structures of α-Fe2O3(0001) Phases determined by LEED Crystallography, G. Ketteler et al., Surf. Rev. Lett. 8 (2001), 661.

16

[52]   S. Thevuthasan, Y. J. Kim, S. I. Yi, S. A. Chambers, J. Morais, R. Denecke, C. S. Fadley, P. Liu, T. Kendelewicz, G. E. Brown Jr.; Surf. Sci. **425**, 276 (1999).
[53]   S. C. Parker, N. H. de Leeuw, S. E. Redfern; Farad. Discuss. **114**, 381 (1999).
[54]   F. Jones, A. L. Rohl, J. B. Farrow, W. van Bronswijk; Phys. Chem. Chem. Phys. **2**, 3209 (2000).
[55]   C. H. Rochester, S. A. Topham; J. Chem. Soc. Faraday Trans. I **75**, 1073 (1979).
[56]   Y. Joseph, G. Ketteler, C. Kuhrs, W. Ranke, W. Weiss, R. Schlögl; Phys. Chem. Chem. Phys. (2001), in print.
[57]   I. Diakanov, I. Khodakovsky, J. Schott, and E. Sergeev; Eur. J. Min. **6**, 967 (1994).
[58]   X.-G. Wang, private communication.
[59]   C. M. Eggleston; Am. Mineral. **84**, 1061 (1999).
[60]   I. Batyrev, A. Alavi, M. W. Finnis; Farad. Discuss. **114**, 33 (1999).
[61]   J. Toofan and P.R. Watson; Surf. Sci. **401**, 162 (1998).
[62]   C. Verdozzi, D. R. Jennison, P. A: Schultz, M. P. Sears; Phys. Rev. Lett. **82**, 799 (1999).
[63]   I. Manassidis, A. de Vita and M.J. Gillan; Surf. Sci. **285**, L517 (1993).
[64]   F. Rohr, M. Bäumer, H.-J. Freund, J.A. Mejias, V. Staemmler, S. Müller, L. Hammer and K. Heinz; Surf. Sci. **372**, L291 (1997); Surf. Sci. **389**, 391 (1997).
[65]   P. Guénard, G. Renaud, A. Barbier, M. Gautier-Soyer; Surf. Rev. Lett. **5**, 321 (1997).
[66]   C. Rehbein, F. Michel, N. M. Harrison, A. Wander; Surf. Rev. Lett **5**, 337 (1998).
[67]   E. Wassermann, J. R. Rustad, A. R. Felmy, B. P. Hay, J. W. Halley; Surf. Sci. **385**, 217 (1997).